CONCRETE LIBRARY OF JSCE NO.3, JUNE 1984

STUDIES ON DEFORMATION AND CRACK OF REINFORCED CONCRETE FLEXURAL MEMBERS UNDER LOW TEMPERATURE

(Reprint from Proceedings of JSCE, No.329, January 1983)

Ryoichi SATO

Yukio AOYAGI

SYNOPSIS

A nonlinear analytical method of deformations as well as crack widths of reinforced concrete members under very low temperatures, which is based on bond stress−slip relationships and is capable of estimating systematically the behaviours from the commencement of cracking up to the state of yielding in steel without assuming predetermined crack spacing. In this analysis, basic differential equations derived in the zone of acting bond stress is solved numerically under the given boundary conditions. Comparisons of analytical and experimental results show that the present method gives a good accuracy of prediction.

R. Sato is an associate professor of civil engineering at Utsunomiya University, Tochigi, Japan. He received his Doctor of Engineering Degree in 1982 from Tokyo Institute of Technology. His research interests include the analysis of deformation and cracking behaviours, thermal stresses of reinforced concrete members induced by temperature gradient. He is a member of JCI Research Committee on cracking. He is also active in JSCE Research Committee on airport pavement.

Y. Aoyagi is the head of material mechanics section at Civil Engineering Laboratry, Central Research Institute of Electric Power Industry, Chiba, Japan. He received his MS in 1964 and his Doctor of Engineering Degree in 1974 from Tokyo University, Tokyo, Japan. His research interests include design and construction of concrete containments for nuclear reactors, in−ground tanks for strage of LNG, prediction of cracking and deformational behaviours of reinforced concrete members under extremely low and elevated temperatures, creep, shrinkage and thermal effects on concrete structures, etc.. He is a member of ACI and has published several papers on the J Division of the proceedings of SMiRT Conferences.

STUDIES ON DEFORMATION AND CRACK OF REINFORCED CONCRETE FLEXURAL MEMBERS UNDER LOW TEMPERATURE

By Ryoichi SATO and Yukio AOYAGI***

1. INTRODUCTION

Cylindrical walls as well as base slabs of reinforced concrete (RC) tanks for liquefied natural gas (LNG) are cooled down to as low as −50∼−70°C due to the effect of LNG which has the boiling point of −162°C, even if the inside face of the container is lined with thermal insulation.

It is well known that the mechanical behaviors of water-saturated RC members under such temperature conditions are markedly different from those observed under normal temperatures (N.T.), owing to the increased properties of concrete and bond strengths as a result of freezing[1]. Especially, the rigidities of RC members have been observed to increase remarkably because the contribution of concrete between adjacent cracks in carrying stress becomes conspicuous due to the increase of tensile as well as bond strengths of concrete under low temperature (L.T.)[2],[3].

When the limit state design, which is likely to be adopted in Japan in the near future, is to be applied also to RC structure exposed to L.T., the structures or members must be checked in the light of deformational as well as cracking behaviors. However, little has been investigated quantitatively except for a few papers written from a phenomenological point of view.

Several empirical formulas dealing with moment-average curvature relationships of RC members have been proposed by Branson[4], Ban[5], Yu *et al.*[6], Beeby *et al.*[7], Sakai *et al.*[8] as well as Rao *et al.*[9]. With some modifications Branson's and Rao's proposals are adopted in ACI[10] and CEB-FIP Codes[11], respectively. Although these formulas are simple and practical in the case of applying to RC members under N.T., more investigations as well as modifications should be made before they could be applicable to RC members under L.T., because such influential factors as bond and strength of concrete, which affect the deformational properties of RC members, have as yet not been fully clarified.

Muguruma and Morita[12] as well as Tsimbikakis[13] developed methods of evaluation for moment-average curvature relationships based on hypothetical averaged sections which give average strains in the reinforcements. Muguruma and Morita calculated the average strains in reinforcements of RC tension members not only empirically but also analytically[14]. This method is, however, not intended for the analysis of RC members under L.T.

As for crack widths of RC members, a number of proposals have so far been made based on the test results obtained under the condition of N.T. For example, CEB-FIP Code[11] as well as Morita's formula[15] employ experimental equations incorporating crack spacings and average strains in reinforcements as main parameters. However, the applicability of these formulas is restricted to what is called "stabilized region", in which RC members cease to develop additional new cracks. Whereas it rather frequently occurs that although RC members under L.T. have a very small number of cracks in "unstable region", the reinforcements are subjected to considerably high stresses.

Having the above mentioned situations in mind, in the framework of the present study, we proposed a nonlinear analytical method of deformations as well as crack widths of RC members, which is based on bond stress-slip relationships and is capable of estimating systematicaliy the behaviors from the commencement of cracking up to the state of yielding in steel without assuming preditermined crack spacings. In this analysis, basic differential equations derived in the zone of acting bond stress is solved numerically under the given boundary conditions. The present theory is only applicable to the cases, in which

idealized RC flexural members are subjected to constant bending along their axes. The main features of the analysis are summarized as follows;

i) It can consider nonlinearity of stress-strain relationships of concrete under both compressive and tensile stresses.

ii) It can incorporate what is called "prestress effect" which is caused by the difference of thermal contraction of concrete and steel under L.T.

iii) It can take into consideration the softening region of bond stress-slip curves as well as bond failure.

iv) It can also deal with the problem of bending combined with axial forces.

2. MATERIAL PROPERTIES

In this section material properties are presented, which were assumed for the analysis. Concrete was considered to be water-saturated as was representative in the concrete of RC members.

(1) Stress-Strain Relationships of Concrete

For the range of temperatures and concrete strengths considered, stress-strain relationships for uniaxial compression and tension were represented as the following parabolic equations;

$$\left.\begin{aligned} \text{Compression:}\quad & \sigma_{cc}/\sigma_{cu}=1-(1-\epsilon_{cc}/\epsilon_{cu})^2 \\ \text{Tension:}\quad & \sigma_{ct}/\sigma_{tu}=1-(1-\epsilon_{ct}/\epsilon_{tu})^2 \end{aligned}\right\} \cdots(1)$$

where

σ_{cc}, σ_{ct}: compressive and tensile stresses
σ_{cu}, σ_{tu}: compressive and tensile strengths
ϵ_{cc}, ϵ_{ct}: compressive and tensile strains
ϵ_{cu}, ϵ_{tu}: compressive and tensile strains at the maximum stresses (in the following refered to as compression and tensile ultimate strains)

Compressive strengths under L.T. were determined as the sum of measured strengths under N.T. and the incremental strengths $\Delta\sigma_{cu}$ under L.T. proposed by Okada *et al.*

$$\{\sigma_{cu}\}_T=\{\sigma_{cu}\}_{N.T.}+\Delta\sigma_{cu} \cdots\cdots(2)$$

$$\Delta\sigma_{cu}=54-8.64T-0.0276T^2$$

$$-10°C\geqq T\geqq -100°C,\quad 0.38\leqq W/C\leqq 0.63$$

where

T: algebraic value of temperature, °C

The above equation was extrapolated down to −120°C and no strength margins were added above 0°C.

Ultimate compressive strains were assumed according to the strength classes and the temperatures investigated as follows;

high strength concrete (H S.C.)
$\epsilon_{cu}=3\,000\,\mu$ (N.T.)
normal strength concrete (N.S.C.)
$\epsilon_{cu}=2\,000\,\mu$ (N.T.)

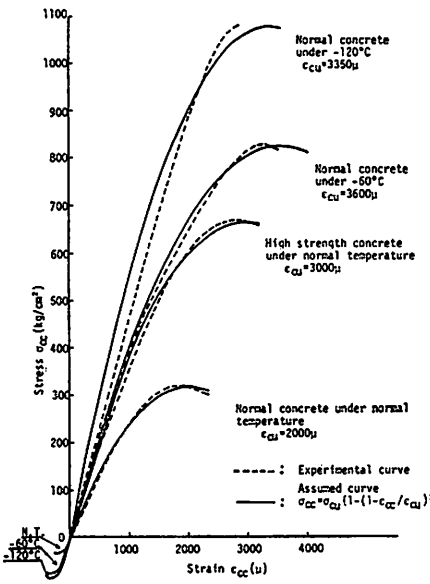

Fig. 1 Comparison of experimental and assumed stress-strain curves of concrete under normal and low temperatures.

normal strength concrete (N.S.C.)
$\epsilon_{cu}=3\,600\,\mu$ (− 60°C)
normal strength concrete (N.S.C.)
$\epsilon_{cu}=3\,350\,\mu$ (−120°C)

Comparisons of the assumed stress-strain curves with the experimentals are made in Fig. 1, which shows a fairly good agreement between the two. In this figure are also drawn stress-strain curves for tension, which were assumed to be analogous to those under compression. Tensile strengths of concrete under L.T. were given by the following equations[16];

$$\{\sigma_{cu}\}_T=\{\sigma_{tu}\}_{N.T.}+\Delta\sigma_{tu},\quad 0°C\geqq T\geqq -120°C \cdots(3)$$

$$T=-8.17\times10^{-4}\Delta\sigma_{tu}^3+0.0155\Delta\sigma_{tu}^2-0.363\Delta\sigma_{tu}$$

$\Delta\sigma_{tu}$: tensile strength increments under L.T.

(2) Bond Stress-Slip Relationships

Bond stress-slip relationships, which are fundamental in the present analysis, were constructed based on the measured strain distributions in reinforcements along RC beams tested flexurally under N.T. as well as −60°C[16]. In this case relative slips were obtained without subtracting the concrete deformations at the level of reinforcements.

As a basis for bond stress-slip ($\tau_x-\delta_x$) curves the following empirical formula proposed by Muguruma, Morita and Tomita[17] was adopted, which seemed appropriate to express the descending branch of the $\tau_x-\delta_x$ curve;

$$\frac{\tau_x}{\tau_{max}}=e\frac{\ln\{(e-1)\delta_x/\delta_{max}+1\}}{(e-1)\delta_x/\delta_{max}+1} \quad \cdots\cdots(4)$$

The parameters determining the bond stress-slip curves, that is, maximum bond stress τ_{max} and the slip at τ_{max}, δ_{max}, were assumed as follows, making reference to the results obtained by Muguruma *et al.*[17], Nilson[21] and also taking into account the concrete strength classes, temperatures under consideration[16];

H.S.C.(N.T.): $\tau_{max}=80$ kg/cm² (7.84 MPa), $\delta_{max}=0.006$ cm, $\delta_u=0.02$ cm

N.S.C.(N.T.): $\tau_{max}=60$ kg/cm² (5.88 MPa), $\delta_{max}=0.006$ cm, $\delta_u=0.02$ cm

N.S.C.(−60°C): $\tau_{max}=180$ kg/cm² (17.64 MPa), $\delta_{max}=0.012$ cm, $\delta_u=0.026$ cm

N.S.C.(−120°C): $\tau_{max}=250$ kg/cm² (24.50 MPa), $\delta_{max}=0.018$ cm, $\delta_u=0.032$ cm

δ_u, the ultimate slip corresponding to bond failure at which bond stress drops to zero was assumed in this study on the supposition that bond failure is caused by local deterioration in the zone near the cracked section and the crack development along reinforcement due to wedging action of its transverse ribs[22].

In **Fig. 2** the assumed curves for bond stress-slip were compared with the experimental plots, which were obtained by the tests of four cases of RC beams with almost the same amount of reinforcements but for the difference of the diameters of bars (16 mm and 32 mm) under both N.T. and −60°C as well as at the two different levels of loading. Experimental values herein

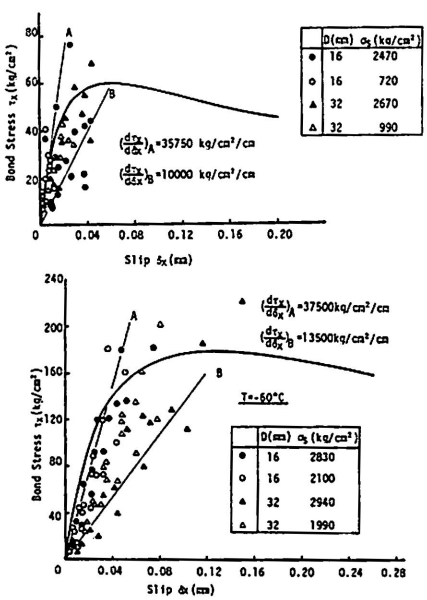

Fig. 2 Bond stress-slip relationships under normal and low temperatures.

were those up to the τ_{max}. The bond stresses may be regarded to be a function of only bond slip values, independent of temperature conditions, diameters of bars as well as stress levels in reinforcements, which suggests the validity of adoption of equation (4).

The assumed curves in **Fig. 2** seem to have steeper tangents than those of experimental values. This may be attributable to aforementioned negligence of concrete tensile deformations between adjacent cracks. How to relate the $\tau_x-\delta_x$ curves to the crack widths to be considered is a controversial problem in which the out-of-plane deformation is to be taken into account. However, in the present study the assumed $\tau_x-\delta_x$ curves may be regarded as related to the crack widths averaged through the thickness of beams.

3. PRINCIPLES OF NONLINEAR ANALYSIS

Basic equations were derived for the case of RC beams with rectangular section reinforced with two layers of tension bars.

(1) Assumptions

Following basic assumptions were made for the analysis of deformational as well as cracking characteristics of RC members subjected to flexural moment combined with axial force.

i) Concrete is homogeneous along the member.

ii) The principle of "plane section remains plane" holds with respect to concrete in compression and tensile reinforcements.

iii) Strain of concrete in tension zone is proportional to the distance from neutral axis.

iv) Widths and spacings of cracks are identical for all cracks in a beam. The crack spacing is defined as the length obtained by dividing the distance considered by the number of cracks.

v) Axial force is assumed to be constant.

vi) Crack occurs when the strain in concrete at the extreme tensile fiber reaches the tensile ultimate strain of concrete.

vii) The stress-strain state of bond failure zone is assumed to be the same as that of cracked section and the effect of concrete tension is neglected. In the case of two layered arrangement of reinforcement the lengths of bond failure for the two layers are assumed to be identical.

viii) Bond stress-slip relationship of Eq. (4) is available independent of locations along reinforcement.

The signs of variables appearing in the follow-

ing equations are defined as minus when related to compression or contraction, and as plus when related to tension or extension.

(2) Formulation of Basic Equations

The internal mechanisms of cracked RC members subjected to bending moment are basically classified into four cases indicated in **Fig. 3**, according to the combinations of presence and absence of perfectly bonded zone as well as bond failure zone, that is;

- (I) Presence of perfect bond zone (PBZ) and absence of bond failure zone (BFZ). (CASE I)
- (II) Presence of both PBZ and BFZ. (CASE II)
- (III) Absence of both PBZ and BFZ. (CASE III)
- (IV) Absence of PBZ and presence of BFZ. (CASE IV)

Stresses and strains of the sections in PBZ as well as BFZ can easily evaluated by the conventional analytical procedures. Therefore, estimation for the deformation of RC members is only possible when the distribution of curvatures in the active bond regions is accurately evaluated.

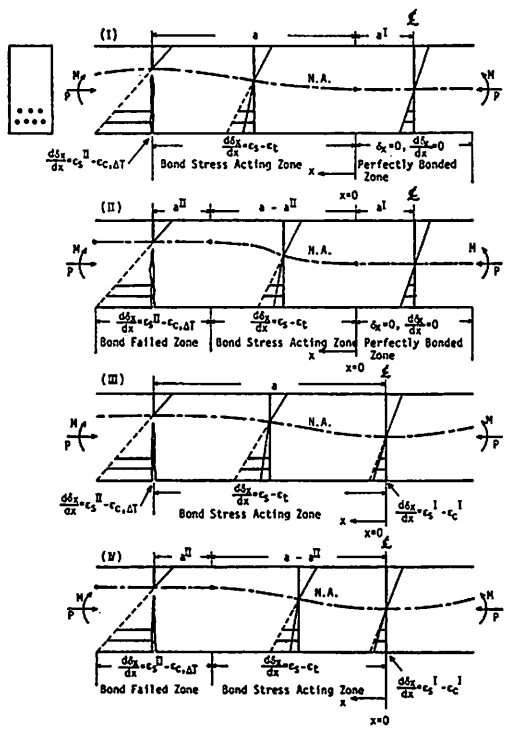

Fig. 3 Four internal mechanisms of RC flexural member.

The distributions of stress related strain, stress as well as resultant forces in concrete and steel at the section located at the distance of x measured from the section at which bond stress begins to act ($x=0$) are illustrated in Fig. 4 together with those at the section of $x+dx$ within the range of active bond zone. The stress related strain $\varepsilon_{co}(z)$ in compression zone and $\varepsilon_{ct}(z)$ in tension zone as well as the pertinent stresses $\sigma_{co}(z)$ and $\sigma_{ct}(z)$ at the distance z (always positive) from the neutral axis, together with stresses in steel σ_{s2} and σ_s, for the section x, can be expressed as functions of three variables ε_s, ε_t and y, using the conditions of strain compatibility of Eq. (5) and stress-strain curves of Eq. (1).

o Compatibility conditions;

$$\left.\begin{aligned} -\frac{\varepsilon_c-\varepsilon_{c,\Delta T}}{y}&=-\frac{\varepsilon_{co}(z)}{z}=\frac{\varepsilon_{s2}-\varepsilon_{c,\Delta T}}{d_2-y}\\ &=\frac{\varepsilon_s-\varepsilon_{c,\Delta T}}{d-y}\quad\text{(Assum. ii)}\\ \frac{\varepsilon_{ct}(z)}{z}&=\frac{\varepsilon_{t2}-\varepsilon_{c,\Delta T}}{d_2-y}=\frac{\varepsilon_t-\varepsilon_{c,\Delta T}}{d-y}\quad\text{(Assum. iii)}\end{aligned}\right\}\quad\cdots\cdots(5)$$

where

- ε_{s2}, ε_s: Total strains in lower and upper layers of tension steel due to axial force, temperature drop and bending moment
- ε_c, ε_t, ε_{t2}: Total strains in concrete at extreme compression fiber, and at the same levels of lower and upper tension reinforcements, respectively, due to axial force, temperature drop and bending moment
- $\varepsilon_{c,\Delta T}$, $\varepsilon_{s,\Delta T}$: Free contraction of concrete and steel due to temperature drop, $\varepsilon_{c,\Delta T}=\alpha_c\Delta T$ and $\varepsilon_{s,\Delta T}=\alpha_s\Delta T$, α_c and α_s: averaged thermal contraction coefficients of concrete (10.38×10^{-6}/°C at −60°C, 9.29×10^{-6}/°C at −120°C) and steel (12.25×10^{-6}/°C at −60°C, 11.26×10^{-6}/°C at −120°C) from room to low temperature considered[20], ΔT: temperature drop from room to low temperature considered
- d, d_2: distances of centroids of lower and upper tension steels from the extreme compression fiber
- y: distance of the extreme compression fiber from neutral axis at the section x
- E_s: Elastic modulus of steel

At the section with the coordinate x, the following equilibriums are satisfied with respect to axial force and bending moment;

$$P=C+T_C+T_{SS}\quad\cdots\cdots(6)$$

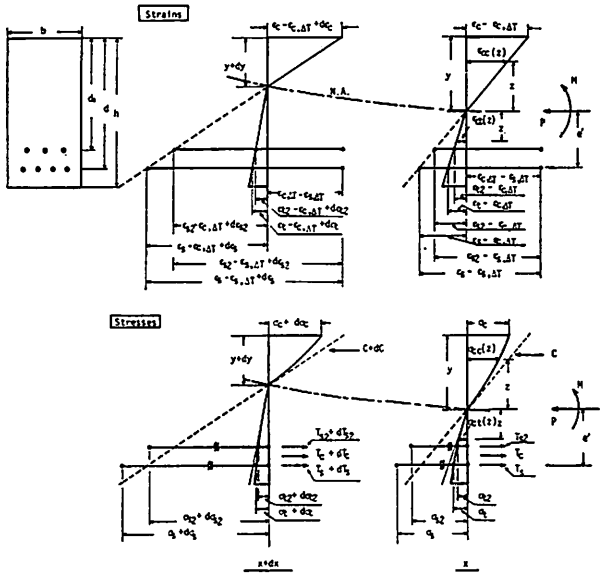

Fig. 4 Changes of stress and strain distributions as well as residual forces for an length of dx.

$$M=Mc+M_{TC}+M_{TS}-Pe' \quad \cdots\cdots(7)$$

where

- P: Axial force (in the case of absence of axial force, $P=0$)
- M: Acting moment
- C: Resultant compressive force in concrete
- Tc: Resultant tensile force in concrete
- Tss: Resultant tensile force in reinforcements
- Mc: Resisting moment of C about the level of the lower reinforcement
- M_{TC}: Resistng moment of Tc about the level of the lower reinforcement
- M_{TS}: Resisting moment of tensile force in the upper reinforcement about the level of the lower reinforcement
- e': Distance between the point of action of axial force and the centroid of lower reinforcement

The above force and moment can be written as follows;

$$C=b\int_0^{y}\sigma_{cc}(z)dz=Q_{C1}(y)\epsilon_s^2+Q_{C2}(y)\epsilon_s+Q_{C3}(y)$$

$$Tc=b\int_0^{h-y}\sigma_{ct}(z)dz-A_s\sigma_{ct}(d-y)-A_{s2}\sigma_{ct}(d_2-y)$$
$$=Q_{TC1}(y)\epsilon_t^2+Q_{TC2}(y)\epsilon_t+Q_{TC3}(y)$$

$$T_{SS}=T_S+T_{S2}=A_s\sigma_s+A_{s2}\sigma_{s2}$$
$$=Q_{TS1}(y)\epsilon_s+Q_{TS2}(y)$$

$$Mc=b\int_0^{y}\sigma_{cc}(z)(d-y+z)dz=P_{C1}(y)\epsilon_s^2$$
$$+P_{C2}(y)\epsilon_s+P_{C3}(y)$$

$$M_{TC}=b\int_0^{h-y}\sigma_{ct}(z)(d-y-z)dz-A_{s2}\sigma_{ct}$$
$$\cdot(d_2-y)(d-d_2)$$
$$=P_{TC1}(y)\epsilon_t^2+P_{TC2}(y)\epsilon_t+P_{TC3}(y)$$

$$M_{TC}=A_{s2}\sigma_{s2}(d-d_2)=P_{TS1}(y)\epsilon_s+P_{TS2}(y)$$

where

- T_S: Tensile force in lower reinforcement
- T_{S2}: Tensile force in upper reinforcement
- A_s: Cross sectional area of lower reinforcement
- A_{s2}: Cross sectional area of upper reinforcement

The functions of $Q_{C1}(y)$, $Q_{C2}(y)$, etc., do not have any physical meaning, but indicate the function of only "y". About the details of these functions, see reference[16].

Based on the equilibrium conditions of (6) and (7), ϵ_s and ϵ_t may be determined if the value of y is given, which means both ϵ_s and ϵ_t are the functions of y, as follows;

$$H_1(y)\epsilon_s^4+H_2(y)\epsilon_s^3+H_3(y)\epsilon_s^2$$
$$+H_4(y)\epsilon_s+H_5(y)=0 \quad \cdots(8)$$

$$\epsilon_t=\Big[-Q_{TC2}(y)$$
$$+\sqrt{\left(\begin{matrix}Q_{TC2}(y)-4Q_{TC1}(y)\{F_1(y)\}\\ \cdot\epsilon_s^2+F_2(y)\epsilon_s+F_3(y)\}\end{matrix}\right)}\Big]\Big/\{2Q_{TC1}(y)\}$$
$$\cdots\cdots(9)$$

The above equilibriums must also hold at the point of $x+dx$, that is, infinitesimal dx apart from the point of x. Therefore, the following equiliriums must be satisfied with respect to infinitesimal increments of force and moment related to dx;

$$dC+dTc+dT_{SS}=0 \quad \cdots\cdots(10)$$
$$dMc+dM_{TC}+dM_{TS}=0 \quad \cdots\cdots(11)$$

Each increment is written as follows;

$$dC=\frac{\partial C}{\partial y}dy+\frac{\partial C}{\partial \epsilon_s}d\epsilon_s$$

$$dTc=\frac{\partial Tc}{\partial y}dy+\frac{\partial Tc}{\partial \epsilon_t}d\epsilon_t$$

$$dT_{SS}=\frac{\partial T_{SS}}{\partial y}dy+\frac{\partial T_{SS}}{\partial \epsilon_s}d\epsilon_s$$

$$dMc=\frac{\partial Mc}{\partial y}dy+\frac{\partial Mc}{\partial \epsilon_s}d\epsilon_s$$

$$dM_{TC}=\frac{\partial M_{TC}}{\partial y}dy+\frac{\partial M_{TC}}{\partial \epsilon_t}d\epsilon_t$$

$$dM_{TS}=\frac{\partial M_{TS}}{\partial y}dy+\frac{\partial M_{TS}}{\partial \epsilon_s}d\epsilon_s$$

All the above incremental values are also considered to be the function of y. Substituting these increments into Eqs. (10) and (11), the following two incremental equations with the coefficients of the function of y are obtained;

$$\alpha_1(y)d\epsilon_s+\alpha_2(y)dy+\alpha_3(y)d\epsilon_t=0 \quad \cdots\cdots(12)$$

$$\beta_1(y)d\varepsilon_s+\beta_2(y)dy+\beta_3(y)d\varepsilon_t=0 \quad \cdots\cdots(13)$$

where

$$\alpha_1(y)=\frac{\partial(C+T_{ss})}{\partial\varepsilon_s} \qquad \beta_1(y)=\frac{\partial(M_\sigma+M_{TS})}{\partial\varepsilon_s}$$

$$\alpha_2(y)=\frac{\partial(C+T_\sigma+T_{ss})}{\partial y} \qquad \beta_2(y)=\frac{\partial(M_\sigma+M_{T\sigma}+M_{TS})}{\partial y}$$

$$\alpha_3(y)=\partial T_\sigma/\partial\varepsilon_t \qquad \beta_3(y)=\partial M_{T\sigma}/\partial\varepsilon_t$$

Solving Eqs. (12) and (13) simultaneously, they are reduced to the following simple form;

$$d\varepsilon_s=Q(y)dy \quad \cdots\cdots(14)$$

$$d\varepsilon_t=G(y)d\varepsilon_s \quad \cdots\cdots(15)$$

where

$$Q(y)=\frac{\alpha_3(y)\beta_2(y)-\alpha_2(y)\beta_3(y)}{\alpha_1(y)\beta_3(y)-\alpha_3(y)\beta_1(y)}$$

$$G(y)=\frac{\alpha_2(y)\beta_1(y)-\alpha_1(y)\beta_2(y)}{\alpha_3(y)\beta_2(y)-\alpha_2(y)\beta_3(y)}$$

Because the Eqs. (14) and (15) are obtained corresponding to a infinitesimal distance increment dx along member axis, they can be divided by dx;

$$d\varepsilon_s/dx=Q(y)\cdot(dy/dx) \quad \cdots\cdots(16)$$

$$d\varepsilon_t/dx=G(y)\cdot(d\varepsilon_s/dx) \quad \cdots\cdots(17)$$

On the other hand, infinitesimal bond slip between steel and concrete at the level of lower bar $d\delta_x$ for the length of dx can be expressed as the difference of strains between the two materials at the same level[18];

$$d\delta_x=(\varepsilon_s-\varepsilon_t)dx \quad \therefore \quad d\delta_x/dx=\varepsilon_s-\varepsilon_t$$

Further differentiating both sides of the above equation with respect to x, we obtain;

$$d^2\delta_x/dx^2=d\varepsilon_s/dx-d\varepsilon_t/dx \quad \cdots\cdots(18)$$

Applying the relationship of Eq. (17) for $d\varepsilon_s/dx$ and $d\varepsilon_t/dx$, the term $d\varepsilon_t/dx$ can be eliminated;

$$d^2\delta_x/dx^2=\{1-G(y)\}d\varepsilon_s/dx \quad \cdots\cdots(19)$$

As tensile stress in steel is transfered to concrete through bond stress, equilibrium condition must be satisfied between the changes of bond and steel stresses for infinitesimal length of dx;

$$A_s d\sigma_s=U_s\tau_x dx \quad \therefore \quad d\sigma_s/dx=U_s/A_s\cdot\tau_x$$

$$\therefore \quad d\varepsilon_s/dx=U_s/A_sE_s\cdot\tau_x \quad \cdots\cdots(20)$$

where

U_s: Total perimeter of lower bars

Substituting the relationship of Eq. (20) into (19) we obtain the following basic differential equation;

$$d^2\delta_x/dx^2=U_s/A_sE_s\{1-G(y)\}\tau_x \quad \cdots\cdots(21)$$

As the formation of this equation implys, it holds for arbitrary type of function of $\tau_x-\delta_x$ relationship. The above equation is also considered to be a "basic bond equation" for flexural members as compared with that for bond specimens or axial tension members[19], which does not retain the coefficient function of $G(y)$.

Since as mentioned previously, bond stress-slip curve proposed by Muguruma *et al.* is adopted in the present study, putting Eq. (4) into Eq. (21), the following nonlinear differeintal equation of second order is obtained;

$$\left.\begin{aligned}\frac{d^2S_x}{dx^2}&=K_m\{1-G(y)\}\frac{\ln\{(e-1)S_x+1\}}{(e-1)S_x+1}\\&=g(y,S_x)\end{aligned}\right\}\cdots(22)$$

where

$$K_m=\frac{U_s}{A_sE_s}\frac{\tau_{max}}{\delta_{max}}e, \quad S_x=\delta_x/\delta_{max}$$

However, Eq. (22) can not be solved even when the necessary boundary conditions are given, because it contains two unknown valiables S_x and y. Therefore a relationship must be established between the valiables.

Integrating the Eq. (16) from 0 up to x, the steel strain at the point of x, which is also obtained from Eq. (8), can be written as follows;

$$(\varepsilon_s)_{x=x}=(\varepsilon_s)_{x=0}+\int_{y_{x=0}}^{y_{x=x}}Q(y)dy$$

Since strain in concrete at the same level of steel is also given as a function of y as is indicated in Eq. (9), we can connect S_x with y through the following relationship;

$$dS_x/dx=(\varepsilon_s-\varepsilon_t)/\delta_{max}=f(y) \quad \cdots\cdots(23)$$

Consequently, Eq. (22) can be solved so that y satisfies Eqs. (22) and (23) simultaneously.

(3) Boundary Conditions

Although only two boundary conditions suffice to mathematically solve the Eqs. (22) and (23), one more condition is needed to reflect realistically the phenomena peculiar to RC members. More specially speaking, as was shown in **Fig. 3**, in the case of perfect bond zone (PBZ) present, the distance "a" which spans between the starting point of active bond and the nearest cracked section must be determined based on the boundary condition of the cracked section. The condition of bond failure must also be added when such type of failure is to be considered.

When there is no PBZ, in order to determine the depth of neutral axis at the middle section between adjacent cracks $y_x=0$, corresponding to the crack spacing obtained by the calculated number of cracks, similar boundary conditions as mentioned above are necessary.

As will be described in the next paragraph (4), the length of bond failure zone (BFZ) a^{II} is automatically calculated by satisfying the condition below. Mathematical description for boundary conditions governing the internal mechanisms prevailing in RC members can be made in **Fig. 3** according to the combination of presence and absence of PBZ and BFZ (see also **Fig. 3**).

Here. suffixes I and II refer to PBZ and BFZ including cracked section.

(4) Numerical Analysis

Basic equations were numerically solved by the following Runge-Kutta's recurrence formulas;

$$\left.\begin{aligned}
&\{S_x\}_{i+1}=\{S_x\}_i+(K_1+2K_2+2K_3+K_4)/6\\
&\left\{\frac{dS_x}{dx}\right\}_{i+1}=\left\{\frac{dS_x}{dx}\right\}_i+(L_1+2L_2+2L_3+L_4)/6\\
&\left\{\frac{dS_x}{dx}\right\}_{i+1}=f(y_{i+1}) \qquad (i=1, 2, \cdots n)
\end{aligned}\right\} \quad \cdots\cdots(24)$$

where

$K_1=\{dS_x/dx\}_i \Delta x$

$K_2=\left[\left\{\frac{dS_x}{dx}\right\}_i+\frac{L_1}{2}\right]\Delta x$

$K_3=\left[\left\{\frac{dS_x}{dx}\right\}_i+\frac{L_2}{2}\right]\Delta x$

$K_4=\left[\left\{\frac{dS_x}{dx}\right\}_i+L_3\right]\Delta x$

$L_1=g(y_i, \{S_x\}_i)\Delta x$

$L_2=g(y_i+\Delta y/2, \{S_x\}_i+K_1/2)\Delta x$

$L_3=g(y_i+\Delta y/2, \{S_x\}_i+K_2/2)\Delta x$

$L_4=g(y_i+\Delta y, \{S_x\}_i+K_3)\Delta x$

and

Δx: length of each segment ($\Delta x=a/n$), n: number of segments divided ($i=1$ indicates the section at $x=0$ and $i=n+1$ the cracked section), Δy: change of neutral axis depth corresponding to Δx.

The procedures of numerical analysis for deformational and cracking behaviors of RC members based on Eq. (24) are enumerated below, together with a flow chart shown in **Fig. 5**. In the following analysis, the method of average curvature increment was applied to pursue the successive cracking behaviors occuring in the RC beam.

①: Read geometric valuables and material properties etc..

②: Calculate stress·strain conditions and curvature ϕ_{in} induced by "prestress effect".

③: Calculate moment-curvature relationship for given curvature before cracking and then cracking moment.

④: Calculate stress·strain conditions at cracked section for assumed magnitude of moment.

⑤: Calculate stress·strain conditions at perfectly bonded section under the aforementioned moment.

⑥: Calculate stress·strain conditions at the middle section between adjacent cracks.

⑦: Solve the basic equations in the form of recurrence formulas expressed in Eq. (24).

⑧: Judge whether bond failure has occurred or not in the region up to cracked section.

⑨: Judge whether the boundary condition at cracked section is satisfied or not.

⑩: Judge whether calculated average curvature is equal to that given at the start of present step.

⑪: Judge whether new crack develops or not.

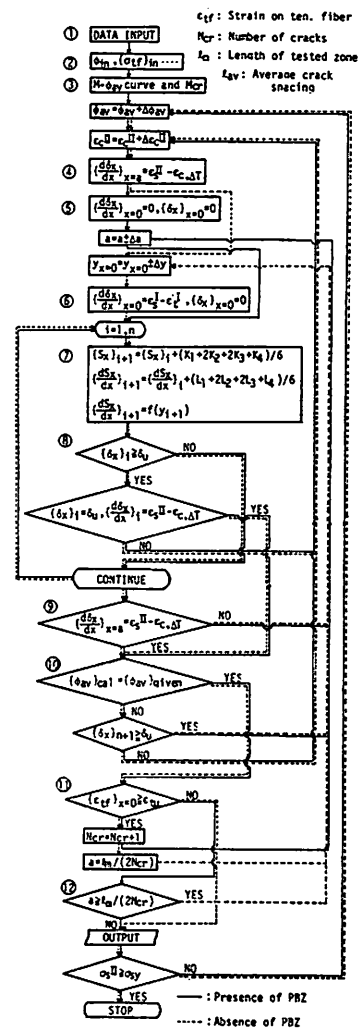

Fig. 5 Flow chart of analytical procedure.

⑫: Judge whether the condition of presence of perfect bond zone is satisfied or not.

As was described in the analytical procedures, y_i and $\{S_x\}_i$ at the section x_i within active bond (ABZ) at the stage when RC member attains the prescribed average curvature can be obtained by solving the Eq. (24). Using the computed y_i and $\{S_x\}_i$ in the Eqs. (4), (8) and (9), the distributions of bond stresses, strains in the lower reinforcement as well as the strains in concrete at the same level of the lower bar along the axis of the member. Moreover, substituting $\{\varepsilon_s\}_i$, $\{\varepsilon_t\}_i$ and y_i into Eq. (5) and then Eq. (1), the distributions of stresses and strains in concrete in the depth of the member may be calculated at arbitrary sections. Based on their values flexural moment can be obtained using Eq. (7). Curva-

ture ϕ_i at arbitrary section can be calculated as follows; $\phi_i=(\{\varepsilon_s\}_i-\varepsilon_{c,sT})/(d-y_i)$. In the case of considering "prestress effect" bending moment induced curvature corresponds to the above value deducted by the contribution due to that effect.

After the stress and strain states as well as curvatures at arbitrary sections of RC members have been determined through the preceeding procedures, average curvatures ϕ_{av} as well as average crack widths w_{av} are calculated according to the four cases defined previously as follows;

CASE I;

$$\phi_{av}=\left\{\phi^{\mathrm{I}}a^{\mathrm{I}}+\frac{1}{2}\sum_{i=1}^{n}(\phi_i+\phi_{i+1})\Delta x\right\}\Big/(a^{\mathrm{I}}+a)$$

$$w_{av}=\sum_{i=1}^{n}\{[\{\varepsilon_s\}_i-\{\varepsilon_t\}_i]+[\{\varepsilon_s\}_{i+1}-\{\varepsilon_t\}_{i+1}]\}\Delta x$$

CASE II;

$$\phi_{av}=\left\{\phi^{\mathrm{I}}a^{\mathrm{I}}+\frac{1}{2}\sum_{i=1}^{n_u-1}(\phi_i+\phi_{i+1})\Delta x+\phi^{\mathrm{II}}a^{\mathrm{II}}\right\}\Big/(a^{\mathrm{I}}+a)$$

$$w_{av}=\sum_{i=1}^{n_u-1}\{[\{\varepsilon_s\}_i-\{\varepsilon_t\}_i]+[\{\varepsilon_s\}_{i+1}-\{\varepsilon_t\}_{i+1}]\}\Delta x+2(\varepsilon_s^{\mathrm{II}}-\varepsilon_{c,sT})a^{\mathrm{II}}$$

CASE III;

$$\phi_{av}=\left\{\frac{1}{2}\sum_{i=1}^{n}(\phi_i+\phi_{i+1})\Delta x\right\}\Big/a$$

$$w_{av}=\sum_{i=1}^{n}\{[\{\varepsilon_s\}_i-\{\varepsilon_t\}_i]+[\{\varepsilon_s\}_{i+1}-\{\varepsilon_t\}_{i+1}]\}\Delta x$$

CASE IV;

$$\phi_{av}=\left\{\frac{1}{2}\sum_{i=1}^{n_u-1}(\phi_i+\phi_{i+1})\Delta x+\phi^{\mathrm{II}}a^{\mathrm{II}}\right\}\Big/a$$

$$w_{av}=\sum_{i=1}^{n_v-1}\{[\{\varepsilon_s\}_i-\{\varepsilon_t\}_i]+[\{\varepsilon_s\}_{i+1}-\{\varepsilon_t\}_{i+1}]\}\Delta x+2(\varepsilon_s^{\mathrm{II}}-\varepsilon_{c,sT})a^{\mathrm{II}}$$

where

n_u: No. of station between two segments at which bond failure starts to occur

$\phi^{\mathrm{I}},\phi^{\mathrm{II}}$: the curvatures in the zones of PBZ and BFZ, respectively

$a^{\mathrm{I}},a^{\mathrm{II}}$: the half lengths of PBZ and BFZ, respectively (see Fig. 3)

For the numerical analysis the number of segmental division was selected to be 500. Although, rigorously speaking, $\varepsilon_s^{\mathrm{I}}=\varepsilon_t^{\mathrm{I}}$ must be implemented in the boundary condition for PBZ, numerically negligible value of $\varepsilon_s^{\mathrm{I}}-\varepsilon_t^{\mathrm{I}}=0.1\times10^{-6}$ was assumed for the sake of numerical analysis.

4. COMPARISONS OF ANALYTICAL AND EXPERIMENTAL RESULTS

(1) Basic Features of Present Analytical Method

As an example to show the basic abilities of authors' analytical method, the calculated distributions of stresses and strains in concrete as well as steel, bond stresses as well as slips, curvatures, position of neutral axis, etc., are illustrated in Fig. 6. The calculations were made on a flexurally tested RC member with percentage of steel $p=1.13\%$ (diameter of bar: 32 mm) and uniform axial compressive stress of $\sigma_{pr}=50$ kg/cm² (4.9 MPa) under −60°C. As can be seen from the figure, the present analysis is possible to evaluate rather quantitatively internal stress and strain distributions in RC members.

In Fig. 7 are also presented, examples of calculations for developments of stresses in steel as well as bond stresses along the axis of RC beams, which were tested under N.T., −60°C and −120°C, together with calculated average crack spacings. The fact that all the crack spacings

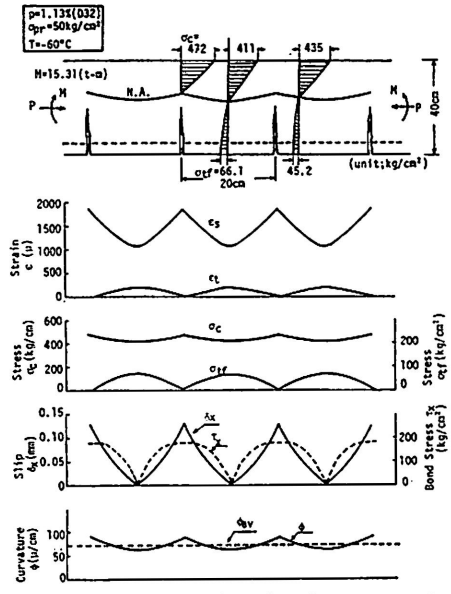

Fig. 6 An example of analyzed stress, strain, slip and cuvrature distributions along longitudinal axis of RC member under −60°C.

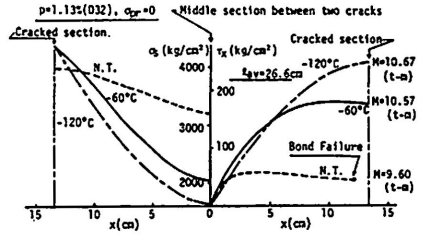

Fig. 7 Typical analyzed distributions of stresses in reinforcing bar and those of bond.

happened to be the same for the above three cases does not necessarily reflect the inability of the proposed method to predict the temperature dependent crack spacings, as is clear from **Table 1.**

As was anticipated by the characteristics of input bond stress-slip curves, the lower the temperature, the rate of increase in reinforcement stress along with the maximum bond stress becomes larger. Under N.T. and −60°C, descending branch of bond stresses can be observed. Especially, under N.T., although defining bond failure as an amount of slip is not necessarily true to actual phenomena of bond, it may be said that at least the zone of bond failure can be displayed by inputting appropriate data for bond stress-slip curves.

(2) Cracking Moment

To accurately compute cracking moment is not only important in the light of confirming the load resisting properties of RC beams but also in view of the fact that cracking moment plays an decisive role in determining deformational behaviors when estimation is to be made such code procedures as ACI and CEB-FIP. In the following characteristics of cracking moment for RC beams are discussed by comparing test results with those obtained by a few varieties of analytical procedures.

As can be seen in **Fig. 8** (I), elastic analysis tends to underestimate cracking moment of RC beams under L.T. even if tensile strength increase of concrete due to freezing effect is taken into account in the calculation. Since the trend seemed attributable mainly to nonlinearity in stress-strain curves of concrete as well as what is called "prestress effect", calculation was performed incorporating the nonlinearity, the results of which are presented in **Fig. 8** (II). The fact that the gradient of regression line for the ratios between measured and calculated cracking moment ($\bar{M}_{cr}$) with respect to reinforcement ratio is almost halved as compared with the former case (**Fig. 8** (I)) indicates an essential role of nonlinearity of concrete. However, the discrepancy between the two values seems still unsatisfactory, which inferred the necessity of considering the second factor, i.e., "prestress effect". **Fig. 8** (III) shows the analytical results when both nonlinearity of concrete and "prestress effect" are taken into consideration. Although $\bar{M}_{cr}$ is a little below unity, the value is almost constant with the changes of reinforcements ratios as well as temperatures, which confirms the validity of the analysis. For instance, the prestress at the extreme tensile fiber were calculated as 17.5 kg/cm² (1.72 MPa) for the beam reinforced with

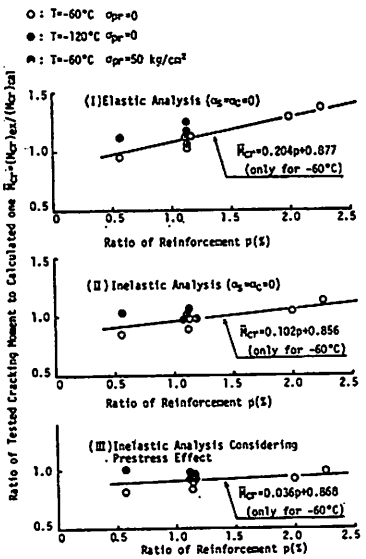

Fig. 8 A comparison of cracking moments under low temperature calculated by three methods.

1.13% steel tested under −120°C and as 16.8 kg/cm² (1.65 MPa) for the beam with reinforcement ratio of 2.26% under −60°C.

(3) Distribution of Strain along Reinforcement

Typically, **Fig. 9** shows comparisons of analytical distributions of strains along reinforcing bars with those obtained by the tests of RC beams with reinforcement ratio of 1.02% subjected to two stages of loading under −60°C.

The above figure indicates that the present analytical method fairly well reflects the rate of strain increase towards cracked section, the number of cracks with the stages of loading, etc. However, some discrepancies may by observed in terms of the manner of strain distributions in the vicinity of cracks and the absolute values of strains. The reason for the former may be explained by the facts that, in this analysis, properties of bond stress-slip curve such as maximum bond stress, slip at bond failure and softening degree of bond stress beyond maximum bond stress, etc. are assumed invariable at every location of reinforcement between adjacent two cracks and that lead wires attached to bars may have deteriorated bond to some extent. The probable explanations for the latter may be that in the analysis contribution of tensile concrete is neglected at the cracked section and that experimentally observed crack spacings were not necessarily uniform. Incorporation of "prestress

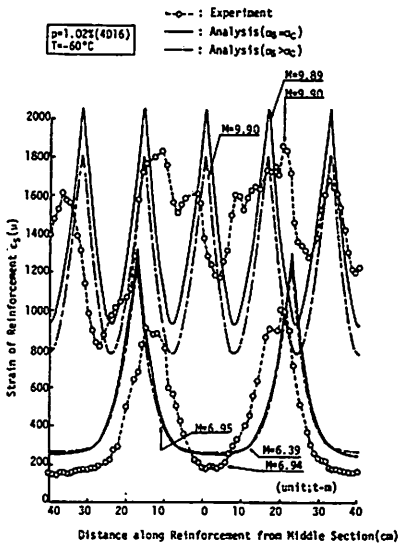

Fig. 9 Typical comparisons of measured and analyzed strain distributions along reinforcement under −60°C.

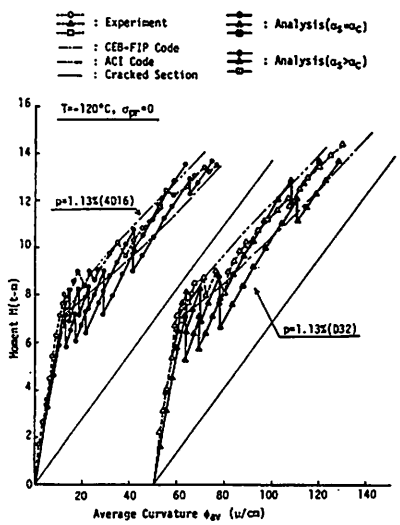

Fig. 10 Comparisons of measured and calculated moment-average curvature relationships.

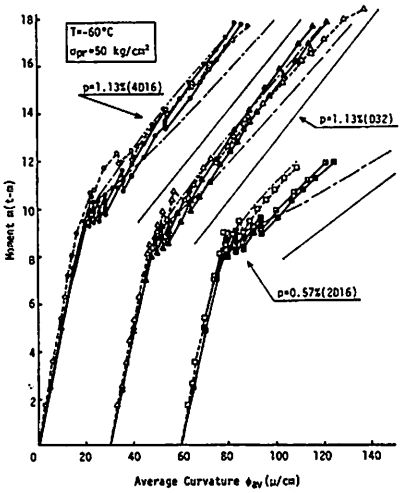

Fig. 11 Comparisons of measured and calculated moment-average curvature relationships.

effect" brings analytical results closer to the experimental values if the comparison is to be made only at the cracked section.

(4) Moment-Average Curvature Relationship

In this section measured moment-average curvature relationships are compared with those calculated by the present method of analysis along with those predicted by ACI as well as CEB-FIP Codes. For the case of CEB-FIP Code, 90% of the strain at cracked section, which is obtained by the authors' method without considering "prestress effect", was assumed in calculating the average curvature. Also, the first cracking moments, which are predicted by the present method without "prestress effect", were used in applying both of the Codes. Such measures were taken because, as was mentioned in section (2), according to elastic calculations as such provided in the Codes, cracking moments are apt to be partially underestimated for the purpose of comparison.

In **Fig. 10** comparisons are made of the two beams with identical reinforcement ratio except for the diameters of bars, 16 mm and 32 mm, which were tested under −120°C.

It can be seen from the figure that all the three methods enable to indicate clearly the contribution of tensile concrete to flexural rigidities, showing a fairly good agreement with test results in terms of tendency. As constructions of the formulas adopted in both Codes imply, it is impossible for them to reflect the phenomena of distinct drop of moment every time a new crack appears.

In contrast the present method can take into account the effect of cracks one by one, being perfectly controlled by deformation, as in the actual test deflection control loading was adopted at the loading points of the beam as shown in **Fig. 14**. Therefore, it pursues the up-and-down of measured curves fairly well. In terms of quantitative evaluations, however, inclusion of "prestress effect", is found to improve the degree

of agreement, especially when temperature is lower.

Fig. 11 corresponds to the cases for RC beams subjected to combined moment and axial force under −60°C. As is shown in this figure, CEB-FIP Code tends to underestimate the moment with increase in curvature for the cases investigated and the tendency is more pronounced as the reinforcement ratio becomes smaller. In applying ACI Code, since no mention is given as to the cases in which axial force is imposed on moment, transformed cracked section moment of inertia obtained from combination of moment and axial force was assumed. It can be seen that ACI Code predicts the test results specifically in this case. The present method, on the other hand, evaluates the deformational behaviors of RC beams with axial force with almost the same accuracy as those without axial force.

(5) Average Crack Spacing

In Table 1 average crack spacings in stabilized crack state obtained by the present analysis were compared with those of experiments as well as those calculated by Morita[15] and CEB-FIP Code[11], for 20 specimens out of 25 tested in the framework of the present study (excluding J, K series and A-3, see Appendix).

Of the three methods investigated CEB-FIP Code gives the fittest results with experimental results under N.T. However, the discrepancies of analytical results among the three methods are not so conspicuous that the authors' proposal may evaluate the crack spacings with almost the same accuracy as those predicted by Morita's as well as CEB-FIP Code in terms of absolute values and scatters.

On the contrary under freezing temperatures, the ratio of experimental results to those calculated by Morita's as well as CEB-FIP Code indicate standard diviations of about 0.4, which are, respectively, 2 and 3.5 times larger than those obtained under N.T. Moreover, CEB-FIP Code estimates average values of crack spacings about 70% smaller than those obtained by experiments. This may be taken as granted, because these practical methods have been so derived based on the experimental data under N.T., that they are not suited for application to the freezing temperature conditions. In the case of present method, however, average values of analytical results almost coincide with those of experiments and the scatters of ratios between calculated and experimental results were reduced to about 1/2 compared with those obtained by Morita's and CEB-FIP Code. The fact that the accuracy of analysis for our method is not almost influenced by temperature conditions may be an indirect evidence for the favorable features of the present method, which is possible to take into account the mechanical as well as bonding properties of concrete independently and also in accordance with the temperature conditions.

Table 1 Comparisons of average crack spacings obtained by experiment with those obtained by Morita, CEB-FIP code and proposed method.

T (°C)	Number of Specimens	Morita		CEB-FIP Code		Proposed Method	
		$\bar{x}$	σ_x	$\bar{x}$	σ_x	$\bar{x}$	σ_x
N.T.	10	0.77	0.20	1.10	0.11	0.79	0.18
−60	8	1.15	0.42	1.71	0.39	1.02	0.23
−120	2						
N.T.	10	0.96	0.38	1.41	0.41	0.91	0.24
−60	8						
−120	2						

$\bar{x}$: Average ratio of measured average crack spacings to calculated ones
σ_x: Standard diviation

(6) Average Crack Width

As a typical example shown in Fig. 12, the crack widths measured in the experiments of RC beams with thick bar of 32 mm, the reinforcement ratio of which was 1.13%, are compared with the analytical results under the temperatures of −60°C. It is clear that Morita's method tends to overestimate crack width. This is due to the fact that Morita's method is apt to overestimate crack spacings when the effective concrete tensile area per a piece of reinforcement Act/m exceeds 100 cm², and that the tendency is extrapolated to the cases of freezing temperatures.

On the other hand, CEB-FIP Code underestimates the experimental results even when the condition attached to average steel strain $\varepsilon_{s,av} \geqq 0.4\varepsilon_s$[11] is observed. The tendency becomes more marked under low temperatures[16]. The main

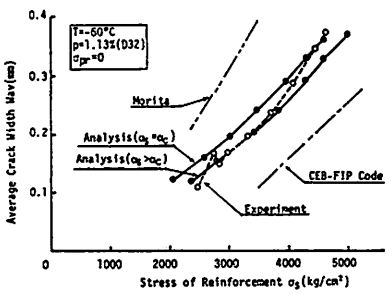

Fig. 12 Typical comparisons of measured and calculated relationships between average crack width and stress of reinforcement.

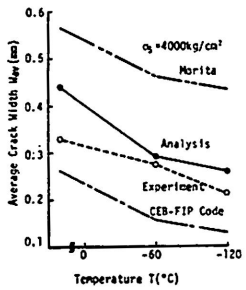

Fig. 13 Typical comparisons of measured and calculated effect of temperature on average crack width.

reason for this, as is indicated in **Table 1**, may be attributed to the fact that according to the Code procedure average crack spacings are also underestimated. Another reason may be due to the fundamental nature of the Code formula, by which average strains in reinforcements are likely to be evaluated smaller because the tensile stresses in reinforcements immediately after first cracking are too high.

The authors' method, however, as was the cases with average crack spacings, gives a good correlation between analytical and experimental results of crack widths, irrespective of temperature conditions, notwithstanding that the method predicts a little larger values than experimental ones. Also, the influence of "prestress effect" can be seen only marginal and therefore may be disregarded in the calculation of average crack widths for the sake of safer evaluations.

Although, as was stated in reference (2), average crack spacings are generally wider at L.T. than at N.T., judging from not only experimental but also analytical considerations, average crack widths are likely to be smaller as the temperature drops, as is indicated in **Fig. 13**. These phenomena can be expressed by the authors' as well as the other two methods investigated. However, the latters, as contrast to the authors', can not calculate the average crack spacings accurately enough to estimate the average crack widths closer to experimental results in quantitative terms.

The summary of comparisons among the three methods of estimations for average crack widths for 20 RC beam specimens tested is tabulated in **Table 2**.

The above mentioned advantages of the authors' method over the other two procedures are confirmed even under N.T. for the ranges of parameters investigated. In the cases of freezing temperatures the two conventional methods show considerably large scatters as against to the authors'. Moreover, while CEB-FIP Code underestimates experimental values to extremely large extent, the degree of underestimation by the authors' is far smaller, which seems to give higher credibility to the authors' method for the prediction of crack widths in the extended ranges of temperatures.

Table 2 Comparisons of average crack width obtained by experiment with those obtained by Morita, CEB-FIP code and proposed method.

T (°C)	Number of Specimens	Morita			CEB-FIP Code			Proposed Method		
		$\tilde{x}$	σ_x	$\tilde{N}$	$\tilde{x}$	σ_x	$\tilde{N}$	$\tilde{x}$	σ_x	$\tilde{N}$
N. T.	10	0.92	0.29	56	1.26	0.29	49	0.99	0.26	56
−60	8 } 10	1.16	0.62	55	1.71	0.54	40	1.21	0.29	55
−120	2 }									
N. T.	10									
−60	8 } 20	1.04	0.50	111	1.46	0.48	89	1.10	0.30	111
−120	2									

$\tilde{x}$: Average ratio of measured average crack width to calculated one
σ_x: Standard diviation
$\tilde{N}$: Number of measured values compared with calculated ones (σ_s^{II}=500~yield at intervals of 500 kg/cm²)

5. CONCLUSIONS

The authors derived a new rational analytical theory for the prediction of deformation as well as cracking behaviors of RC flexural members based on the bond stress-slip relationships between steel and concrete. The following conclusions were drawn from the comparisons of analytical and experimental results;

(1) The following governing differential equation was formulated in the bond active zone of RC members. This equation is able to include such valiables as reinforcement ratios, bar diameters, axial forces concrete strengths and temperature conditions;

$$d^2S_x/dx^2=U_s/A_sE_s\delta_{max}\{1-G(y)\}\tau_x$$
$$dS_x/dx=f(y)$$

where $S_x=\delta_x/\delta_{max}$, $G(y)$ and $Q(y)$ both are functions of only y, which is the depth of neutral axis.

(2) The above equation was solved based on the mathematical boundary conditions, which were classified into the four cases defined by the distributions of the internal bond stress-slip conditions along RC beams. This analytical method was confirmed to be able to predict systematically the deformation as well as cracking behaviors and also the stress-strain states at arbitrary sections of RC beams for the loading stages before first cracking up to yielding in steel.

(3) The authors' developed a rational analytical method to calculate the first cracking mo-

ments of RC beams loaded under freezing temperatures, taking into account the nonlinearity of stress-strain curves for concrete as well as the what is called "prestress effect" which is caused by the difference of thermal contractions between concrete and steel under extremely low temperatures.

(4) By applying the proposed method, strain distributions along RC beams can be predicted fairly truly to the experimental evidences when external moments or average curvatures are given, without previously setting the positions of cracking. This method can also deal with the descending zones of bond stresses and bond failures as well by controlling the types of input bond stress-slip curves.

(5) Comparisons of analytical data with experimental results concerning moment-average curvature relationships showed that the authors' method gives almost the same accuracy of prediction as ACI as well as CEB-FIP Codes, except for that CEB Code tends to underestimate moments of RC beams subjected to axial force under low temperature as curvature proceeds towards the point at which the steel begins to yield. Moreover, the proposed method of analysis was found to be able to represent fairly well the unstable up-and-downs of moment-average curvature relationships, which is especially peculiar to RC beams loaded under low temperature and can not be expressed by the practical formulas such as those adopted in ACI and CEB-FIP Codes. It was also recognized that incorporation of "prestress effect" improves the accuracy of estimation especially when the reinforcement ratios are higher and the temperature is lower.

(6) As for crack spacings of RC members under normal temperatures, the present method is able to evaluate the experimental results with almost the same accuracy as Morita's method and CEB-FIP Code. On the other hand, the authors' method can express the fundamental property of widening crack spacings under lower temperatures so realistically that the accuracy is not impaired even under the condition of freezing temperatures. The above two empirical methods, because of their inability to take into consideration properly the effects of changes of material properties under low temperatures, showed extremely large scatter when compared with experimental results.

(7) Concerning average crack widths, the accuracy of prediction of the authors' method was found to be none the less inferior to Morita's and CEB-FIP Code. As was the case with crack spacings, adaptability of the proposed method to the cases of predicting crack widths under low temperatures was also confirmed superior to the two comparative method in terms of scatters of the ratios between analytical and experimental results. Also, it was recognized that in assessing crack widths as accurately as possible it is imperative for the analytical methods to evaluate crack spacing realistic to phenomena observed in the experiment.

(8) In order to improve the proposed analytical procedures in terms of accuracy, more investigations are needed on the fundamental input data such as the types of bond stress-slip curves includ-

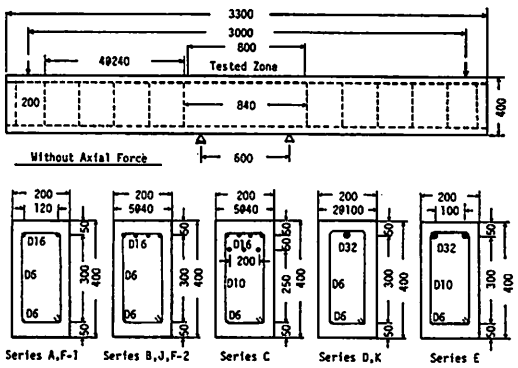

Fig. 14 Typical details of specimens (unit; mm).

Table 3 Properties of RC members.

	p (%)	D (mm)	σ_{pr} (kg/cm²)	T (°C)	Properties of Conc. under N. T. σ_{cu} (kg/cm²)	σ_{bu} (kg/cm²)	σ_{tu}[3] (kg/cm²)	E_c ($\times 10^4$)[1] (kg/cm²)
A-1	0.57	16	0	N.T.	274	45.2	23.3	21.2
2	0.57	16	0	−60	295	52.1	27.4	32.6
3	0.57	16	0	−60	451	44.3	33.2	32.6
B-1	1.13	16	0	N.T.	368	40.6	33.6	31.9
2	1.13	16	0	−60	346	46.7	31.0	29.7
3	1.13	16	0	−120	348	49.4	32.7	30.5
C-1	1.99	16	0	N.T.	256	49.0	23.6	18.8
2	1.99	16	0	−60	301	46.5	28.0	26.0
D-1	1.13	32	0	N.T.	383	45.2	30.8	30.0
2	1.13	32	0	−60	303	41.6	29.3	31.9
3	1.13	32	0	−120	315	41.2	31.3	27.8
E-1	2.26	32	0	N.T.	324	38.6	26.7	31.9
2	2.26	32	0	−60	342	33.5	29.0	30.5
F-1	0.57	16	0	N.T.	684	49.0	44.2	38.7
2	1.13	16	0	N.T.	634	50.5	44.8	36.8
G-1	0.57	16	50	N.T.	347	48.1	36.1	29.2
2	0.57	16	50	−60	378	41.9	26.7	33.0
H-1	1.13	16	50	N.T.	358	48.6	25.5	31.5
2	1.13	16	50	−60	386	43.6	35.7	31.8
I-1	1.13	32	50	N.T.	292	36.1	25.9	29.3
2	1.13	32	0	−60	358	35.0	23.1	38.9
J-1[3]	1.02	16	0	N.T.	327	34.4	26.8	25.2
2[3]	1.02	16	0	−60	355	36.8	30.4	25.6
K-1[3]	1.02	32	0	N.T.	313	35.8	28.4	25.8
2[3]	1.02	32	0	−60	299	34.0	26.4	28.0

1: 1/3 Secant Moduls 2: Size of Specimens $\phi 10 \times 20$ cm
3: Instrumented Bar is used

ing the characteristics of descending branch of bond stress and definition of bond failure as well as contribution of tensile concrete at cracked sections.

6. ACKNOWLEDGEMENTS

The first author wishes to acknowledge the eager encouragement that he received from Professor Dr. S. Nagataki of Tokyo Institute of Technology. Experimental works were carried out at Central Research Institute of Electric Power Industry and numerical computations were performed by the digital computer NEAC-2200/575 of the Computer Center in National Defense Academy.

The authors want to express their gratitude to T. Kanazu, H. Kusaka, M. Kurebayashi and S. Ito for their cooperation in this experiment.

7. APPENDIX: Outline of Experiment[16]

Typical configurations as well as dimensions of RC beams are indicated in **Fig. 14**. Properties of RC beams tested are listed on **Table 3**.

Metric Conversion Factors

1 kg/cm^2=0.098 MPa (=N/mm^2)
1 t-m=9.8 kN·m

REFERENCES

1) Okada, T., M. Imai, Y. Nagasawa, N. Ishikawa and K. Kimura: Flexural Behavior of Concrete Beams at Low Temperature, Concrete Journal, Vol. 15, No. 11, pp. 9~20, Nov. 1977 (in Japanese).
2) Aoyagi, Y. and R. Sato: Mechanical Behaviors of RC Members under Very Low Temperature, Coment·Concrete, No. 334, pp. 18~28, Dec. 1979 (in Japanese).
3) Aoyagi, Y. and R. Sato: Deformation and Cracking Behaviors of Reinforced Concrete Tension Members under Low Temperature, CAJ Review of the 32nd General Meeting, pp. 405~409, 1978.
4) Branson, D. E.: Deflections of Reinforced Concrete Flexural Members, ACI Journal, Proceedings Vol. 63, pp. 637~663, June 1966.
5) Ban, S.: Flexural Rigidity of Reinforced Concrete Beams, Transactions of A.I.J., No. 48, pp. 21~25, March 1954 (in Japanese).
6) Yu, W. W. and G. Winter: Instantaneous and Long-Term Deflections of Reinforced Concrete Beams under Working Load, ACI Journal, Proceedings Vol. 58, No. 1, pp. 29~47, Jan. 1960.
7) Beeby, A. W. and J. R. Hiles: Proposals for the Control of Deflection in the Unified Code, Concrete (London), Vol. 3, No. 3, pp. 101~110, March 1969.
8) Sakai, K. and Y. Kakuta: Moment-Curvature Relationships of Reinforced Concrete Members Subjected to Combined Bending and Axial Force, ACI Journal, Proceedings Vol. 77, No. 3, pp. 189~194, May-June 1980.
9) Rao, P. S. and B. V. Subrahanyam: Trisegmental Moment-Curvature Relations for Reinforced Concrete Members, ACI Journal, Proceedings Vol. 70, No. 5, pp. 346~351, May 1973.
10) ACI 318-77, Building Code Requirements for Reinforced Concrete, 1977.
11) CEB-FIP Model Code for Concrete Structures, 1978.
12) Muguruma, H. and S. Morita: Investigations into the Deformation and the Opening Up of Cracks in Reinforced Concrete Bending Members, Transactions of A.I.J., No. 9, pp. 13~18, Sept. 1963 (in Japanese).
13) Tsimbikakis, S. T.: Short-Term Deflections of Reinforced Concrete Beams, Concrete (London), Vol. 9, No. 1, pp. 34~37, Jan. 1975.
14) Muguruma, H. and S. Morita: Fundamental Study on Bond Between Steel and Concrete (Part 2), Transactions of A.I.J., No. 164, pp. 1~8, Apr. 1967 (in Japanese).
15) Morita, S.: Limitation of Allowable Steel Stress for Crack Width Control in Reinforced Concrete Beams, CAJ Review of the 23rd General Meeting, pp. 552~556, 1969.
16) Sato, R.: Analysis of Deformation and Crack of Reinforced Concrete Flexural Members Subjected to Thermal Loading in the Low Temperature Region, Dissertation Presented at Tokyo Institute of Technology, 1981 (in Japanese).
17) Muguruma, H., S. Morita, and K. Tomita: Fundamental Study on Bond between Steel and Concrete (Part 1), Transactions of A.I.J., No. 131, pp. 1~8, Jan. 1967, No. 132, pp. 1~6, Feb. 1967 (in Japanese).
18) Ödman, Sven T. A.: Slip between Reinforcement and Concrete, RILEM-Symposium on "Bond Crack Formation in Reinforced Concrete", Stockholm, pp. 407~420, 1957.
19) Kosaka, Y. and S. Morita: Reinforced Concrete Structure, Maruzen, pp. 57~59, Dec. 1975 (in Japanese).
20) Japan Gas Association: Tests on Properties of Reinforcing Bars and Concrete under Low Temperature for the Fiscal Year 1977, Report (1), (2), Preservation and Investigation Committee of Storage for Liquified Natural Gas, pp. 1~12 and pp. 1~23, Jan. 1978 (in Japanese).
21) Nilson, A. H.: Internal Measurement of Bond Slip, ACI Journal, Proceedings Vol. 69, No. 7, pp. 439~441, June 1972.
22) Edward, A. D. and P. J. Yannopoulus: Local Bond-Stress to Slip Relationships for Hot Rolled Deformed Bars and Mild Steel Plain Bars, ACI Journal, Proceedings Vol. 76, No. 3, pp. 405~420, March 1979.

(Received January 25, 1982)